arXiv:0906.1146v2 [astro-ph.CO] 6 Jun 2009

Density profiles of dark matter haloes on Galactic and Cluster scales

A. Del Popolo[1,2,3] & P. Kroupa[2]

1 Dipartimento di Fisica e Astronomia, Universitá di Catania, Viale Andrea Doria 6, 95125 Catania, Italy
[2] Argelander-Institut für Astronomie, Auf dem Hügel 71, D-53121 Bonn, Germany
3 Istanbul Technical University, Ayazaga Campus, Faculty of Science and Letters, 34469 Maslak/ISTANBUL, Turkey

ABSTRACT

In the present paper, we improve the "Extended Secondary Infall Model" (ESIM) of Williams et al. (2004) to obtain further insights on the cusp/core problem. The model takes into account the effect of ordered and random angular momentum, dynamical friction and baryon adiabatic contraction in order to obtain a secondary infall model more close to the collapse reality. The model is applied to structures on galactic scales (normal and dwarf spiral galaxies) and on cluster of galaxies scales. The results obtained suggest that angular momentum and dynamical friction are able, on galactic scales, to overcome the competing effect of adiabatic contraction eliminating the cusp. The NFW profile can be reobtained, in our model only if the system is constituted just by dark matter and the magnitude of angular momentum and dynamical friction are reduced with respect to the values predicted by the model itself. The rotation curves of four LSB galaxies from de Blok & Bosma (2002) are compared to the rotation curves obtained by the model in the present paper obtaining a good fit to the observational data. On scales smaller than $\simeq 10^{11} h^{-1} M_{\odot}$ the slope $\alpha \simeq 0$ and on cluster scales we observe a similar evolution of the dark matter density profile but in this case the density profile slope flattens to $\alpha \simeq 0.6$ for a cluster of $\simeq 10^{14} h^{-1} M_{\odot}$. The total mass profile, differently from that of dark matter, shows a central cusp well fitted by a NFW model.

Key words. cosmology–theory–large scale structure of Universe–galaxies–formation

1. Introduction

The structure of dark matter haloes is of fundamental importance in the study of the formation and evolution of galaxies and clusters of galaxies. At the simplest level, dark matter halos form when, in the early Universe, the matter within (and surrounding) an overdense region suffers gravitational retardation, decouples from the Hubble flow, collapses, and in due course, virializes. From the theoretical point of view, the structure of dark matter haloes can be studied both analytically and numerically. A great part of the analytical work done so far is based on the secondary infall model (SIM) introduced by Gunn & Gott (1972), Gott (1975) and Gunn (1977). Calculations based on this model predict that the density profile of the virialized halo should scale as $\rho \propto r^{-9/4}$. Self-similar solutions were found by Fillmore & Goldreich (1984) and Bertschinger (1985), while Hoffman & Shaham (1985) (hereafter HS) studied density profiles around density peaks. More recently modifications of the self-similar collapse model to include more realistic dynamics of the growth process have been proposed (e.g. Avila-Reese et al. 1998; Nusser & Sheth 1999; Henriksen & Widrow 1999; Subramanian et al. 2000; Del Popolo et al. 2000

(hereafter DP2000)). Ryden & Gunn (1987) (hereafter RG87) were the first to relax the assumption of purely radial self-similar collapse by including non-radial motions arising from secondary perturbations in the halo. Numerous authors have emphasized the effect of an isotropic velocity dispersion (thus of non-radial motion) in the core of collisionless haloes. One common result of the previous studies (RG87; White & Zaritski 1992; Avila-Reese et al. 1998; Hiotelis 2002; Nusser 2001; Le Delliou & Enriksen 2003; Ascasibar et al. 2004; Williams et al. 2004) is that larger amount of angular momentum leads to shallower final density profiles in the inner region of the halo. Moreover, baryons have been invoked both to shallow (El-Zant et al. 2001 (hereafter EZ01), 2003; Romano-Diaz et al. 2008) and to steepen (Blumenthal et al. 1986) the dark matter profile.

As previously reported, the structure of dark matter haloes can also be studied through numerical simulations. Quinn, Salmon & Zurek (1986) pioneered the use of N-body simulations to study halo formation and confirmed HS results. More recent studies, (Dubinski & Carlberg 1991, Lemson 1995, Cole & Lacey 1996, Navarro et al. 1996, 1997 (NFW), Moore et al. 1998, Jing & Suto 2000, Klypin et al. 2001, Bullock et al. 2001, Power et al. 2003 and Navarro et al. 2004) found that although the spherically-averaged density profiles of the N-body dark matter halos are similar, regardless of the mass of the halo or the cosmological model, their profiles are significantly different from the single power laws predicted by the theoretical studies. The N-body profiles are characterized by an r^{-3} decline at large radii and a cuspy profile of the form $\rho(r) \propto r^{-\alpha}$, where $\alpha < 2$ near the center. The actual value of the inner density slope α is a matter of some controversy, with NFW suggesting $\alpha = 1$, but with Moore et al. (1998), Ghigna et al. (2000) and Fukushige & Makino (2001) arguing for $\alpha = 1.5$, while Jing & Suto (2000) and Klypin et al. (2001) claimed that the actual value of α may depend on halo mass, merger history, and substructure. Power et al. (2003) pointed out that the logarithmic slope becomes increasingly shallow inwards, with little sign of approaching an asymptotic value at the resolved radii. In that case, the precise value of α, at a given cut-off scale, would not be particularly meaningful. This result has been later confirmed by Hayashi et al. (2003) and Fukushige et al. (2004), and it is predicted by several analytical models (e.g., Taylor & Navarro (2001), Hoeft et al. 2003). Finally, Navarro et al. (2004) proposed a new fitting formula having a logarithmic slope that decreases inward more gradually than the NFW profile.

While numerical simulations universally produce a cuspy density profile, observed rotation curves of dwarf spiral and LSB galaxies seem to indicate that the shape of the density profile at small scales is significantly shallower than what is found in numerical simulations (Flores & Primak 1994; Moore 1994; Burkert 1995; Kravtsov et al. 1998; Salucci & Burkert 2000; Borriello & Salucci 2001; de Blok et al. 2001; de Blok & Bosma 2002; Marchesini et al. 2002; de Blok 2003; de Blok, Bosma & McGaugh 2003). It seems that the data generally favor logarithmic density slopes close to 0.2 (de Blok 2003; de Blok, Bosma & McGaugh 2003; Spekkens et al. 2005).

On cluster scales, X-ray analyses have led to wide ranging results, from $\alpha = 0.6$ (Ettori et al. 2002) to $\alpha = 1.2$ (Lewis et al. 2003) or even $\alpha = 1.9$ (Arabadjis et al. 2002). Ricotti's (2003) N-body simulations suggest that density profile of DM haloes is not universal (in agreement with Jing & Suto 2000; Subramanian et al. 2000; Simon et al. 2003b; Cen et al. 2004; Ricotti & Wilkinson 2004; Ricotti et al. 2007), presenting shallower cores in dwarf galaxies and steeper cores in clusters.

The discrepancy between simulations and observations has been often signaled as a genuine crisis of the CDM scenario and has become known as the "cusp/core" problem. Since LSB galaxies are thought to be ideal for the comparison with theory, as their dynamics are dominated by dark matter with little contribution from baryons (Bothun *et al.* 1997), the discrepancy with simulations is particularly troublesome. The significance of this disagreement, though, remains controversial and different solutions have been proposed. A number of authors attribute the problem to a real failure of the CDM model, or to that of simulations (de Blok et al. 2001a; de Blok, McGaugh, & Rubin 2001b; Borriello & Salucci 2001; de Blok, Bosma, & McGaugh 2003). This has led to suggestions that dark matter properties may deviate from standard CDM and several alternatives have been suggested, such as warm (Colin et al. 2000; Sommer-Larsen & Dolgov 2001), repulsive (Goodman 2000) fluid (Peebles 2000), fuzzy (Hu et al. 2000),

decaying (Cen 2001), annihilating (Kaplinghat et al. 2000), or self-interacting (Spergel & Steinhardt 2000; Yoshida et al. 2000; Dave et al. 2001) dark matter. Others argue that the inconsistency may reflect the finite resolution of the observations that has not been properly accounted for in the analysis of the HI rotation curves (van den Bosch *et al.* 2000; van den Bosch & Swaters 2001; Rhee et al. 2004). Alternatively, it has been suggested that stellar feedback from the first generation of stars formed in galaxies was so efficient that the remaining gas was expelled on a timescale comparable to, or less than, the local dynamical timescale. The dark matter subsequently adjusted to form an approximately constant density core (e.g., Gelato & Sommer-Larsen 1999). This is however unlikely to affect cluster cusps.

Simulations, observations and semi-analytic models agree on outer parts of the haloes' structure the disagreement in the inner regions could be connected to limits in numerical simulations (de Blok 2003; Taylor et al. 2004) or to the fact that dissipationless N-body simulations do not take into account the effects of baryons on dark matter evolution. Interestingly, the amount of central substructure seen in the semi-analytic haloes is consistent with the amount of substructure inferred from strong lensing experiments (Taylor et al. 2004). Thus the semi-analytic haloes might provide a more accurate picture of the spatial distribution of substructure around galaxies even if an analytical method, no matter how sophisticated, will never be able to capture the full extent of complexity of a non-linear process.

Nevertheless the very large amount of work carried out by many researchers to date using N-body simulations has met with limited success in elucidating the physics of halo formation. The reason is due to the fact that the point of force of numerical simulations (namely to capture the full extent of complexity of a non-linear process) is also their weakness: numerical simulations yield little physical insight beyond empirical findings precisely because they are so rich in dynamical processes, which are hard to disentangle and interpret in terms of underlying physics. Analytical and semi-analytical models are much more flexible than N-body simulations (see Williams et al. 2004). So even if analytical models like SIM treat collapse and virialization of halos that are spherically symmetric, that have suffered no major mergers, and that have suffered quiescent accretion, they are worth investigating. One of the most used semi-analytical models is the SIM whose most often questioned assumptions are the spherical symmetry and the absence of peculiar velocities (non-radial motions): in the "real" collapse, accretion does not happen in spherical shells but by aggregation of subclumps of matter which have already collapsed; a large fraction of observed clusters of galaxies exhibit significant substructure (Kriessler et al. 1995). Motions are not purely radial, especially when the perturbation detaches from the general expansion. Nevertheless the SIM gives good results in describing the formation of dark matter haloes, because in energy space the collapse is ordered and gentle, differently from the chaotic collapse that is seen in N-body simulations (Zaroubi, Naim & Hoffman 1996). This is confirmed in other studies (Tóth & Ostriker 1992; Huss, Jain & Steinmetz 1999a,b; Moore et al. 1999). We should also add that analytical and semi-analytical models have some advantages over N-body simulations: a) they are flexible (one can study the effects of physical processes one at a time); b) one can incorporate many physical effects at least in a schematic manner; c) they are computationally efficient (it takes about 10 s to compute the density profile of a given object at a given epoch on a desktop PC, Ascasibar et al. 2007).

In this paper, we shall present an analytical model for haloes formation based on SIM. The model is an extension of the Williams et al. (2004) model to take account of ordered angular momentum, dynamical friction and adiabatic contraction. The model derives the initial shape of proto-halos from the fluctuation spectrum at high redshifts, and halos are endowed with secondary perturbations, which impart random motions to halo particles, as in Williams et al. (2004), and ordered angular momentum. The statistical properties of the secondary perturbations are derived from the same fluctuation power spectrum, and therefore their effects on particles random velocities are treated self-consistently. The ordered angular momentum acquired by the proto-structures is obtained from the tidal interaction of the proto-structure with the neighboring ones and using the theory of random fields. Dynamical friction is calculated according to Kandrup's (1980) approach.

Adiabatic contraction is taken into account using the Blumenthal et al. (1986) model as modified by Gnedin et al. (2004).

The plan of the paper is the following: in Section 2, we introduce the model that shall be used to calculate the density profiles. In Section 3, we show the results of the model, while Section 4 is devoted to conclusions.

2. Model

As shown by the spherical collapse model[1] of Gunn & Gott (1972), a bound mass shell having initial comoving radius x_i will expand to a maximum radius x_m (named apapsis or turn-around radius x_{ta}). As successive shells expand to their maximum radius they acquire angular momentum and then fall in on orbits determined by the angular momentum. Dissipative physics and the process of violent relaxation will eventually intervene and convert the kinetic energy of collapse into random motions (virialization). Following RG87 and R88a,b aproach, we restrict ourselves to halos that form primarily via nearly-smooth accretion of matter, treating collapse and virialization of halos that are spherically symmetric, that have suffered no major mergers, and that have experienced only quiescent accretion of somewhat lumpy material. The most important feature of the original RG87 method is that the dynamical evolution is carried out while conserving angular and radial momenta of individual halo shells. The initial shape of the proto-halos is derived from the fluctuation spectrum at high redshifts, and halos are endowed with secondary perturbations, which impart random motions to halo particles. The statistical properties of the secondary perturbations are derived from the same fluctuation power spectrum, and therefore their effects on particles random velocities are treated self-consistently. Ordered angular momentum is also treated self-consistently as shown in R88a.

It is possible to divide the halo into four regions starting from the outside: in Region (1), furthest from the center of the initial density peak, dark matter particles are beginning to feel the gravitational tug of the central peak and are just starting to fall behind the Hubble flow. Further, in Region (2), the particles are starting to decouple from the Hubble flow and are about to begin collapse. In Region (3) the central density peak dominates the motion of particles; this is the region of infall and shell crossing. Finally, in Region (4), the central part of the density peak, virialization is taking place, or has already been reached. In Region (4), virialization is well underway or is complete. Many analytical solutions in regions (1)-(3) ignore non-radial motions of particles; all orbits are assumed to be purely radial. The calculations carried out in RG87 demonstrate that non-radial motions are very important in determining the outcome in this region. Nonradial motions give particles angular momentum, which prevents them from penetrating to the very center of the halo (confirmed by e.g., Avila-Reese, Firmani & Hernandez (1998), Subramanian et al. (2000), and Hozumi, Burkert & Fujiwara (2000).

In most popular cosmological scenarios the density field soon after recombination can be represented by a Gaussian random field. High density contrast peaks in the field will eventually achieve overdensities of order 1 and enter a non-linear stage of evolution. These peaks will then collapse to form bound structures. We start with one of these peaks, and, for simplicity take it to be spherically symmetric. The peak is divided into a very small central core and many spherically symmetric concentric mass shells, each labeled by its initial comoving distance from the center, x.

The first step in obtaining the density profile, is to calculate the initial density profile arising from a primordial fluctuation, $\overline{\delta}_i(x_i)$. A well known result is the expression for the

---

[1] A slightly overdense sphere, embedded in the Universe, is a useful non-linear model, as it behaves exactly as a closed sub-universe because of Birkhoff's theorem. The sphere is divided into spherical "shells". A spherical "shell" may be defined as the set of particles at a given radius that are all at the same phase in their orbits (see Le Delliou & Henriksen 2003).

radial density profile of a fluctuation centered on a primordial peak of arbitrary height ν:

$$\langle \delta(x) \rangle = \delta_0(x) = \frac{\nu \xi(x)}{\xi(0)^{1/2}} - \frac{\vartheta(\nu\gamma, \gamma)}{\gamma(1 - \gamma^2)} \left[\gamma^2 \xi(x) + \frac{R_*^2}{3} \nabla^2 \xi(x) \right] \cdot \xi(0)^{-1/2} \tag{1}$$

(BBKS; RG87), where x is the comoving separation, $\nu = \delta(0)/\sigma^2$ is the height of a density peak, $\xi(r)$ is the two-point correlation function:

$$\xi(x) = \frac{1}{2\pi^2 x} \int_0^\infty P(k) k \sin(kx) dk \tag{2}$$

γ and R_* are two spectral parameters (see BBKS) and $\vartheta(\nu\gamma, \gamma)$ is given in BBKS.

The CDM spectrum used in this paper is that of BBKS (equation (G3)), with transfer function:

$$T(k) = \frac{[\ln(1 + 2.34q)]}{2.34q} \cdot [1 + 3.89q + (16.1q)^2 + (5.46q)^3 + (6.71)^4]^{-1/4} \tag{3}$$

where $q = \frac{k\theta^{1/2}}{\Omega_x h^2 \text{Mpc}^{-1}}$. Here $\theta = \rho_{\text{er}}/(1.68\rho_\gamma)$ represents the ratio of the energy density in relativistic particles to that in photons ($\theta = 1$ corresponds to photons and three flavors of relativistic neutrinos). The spectrum is connected to the transfer function through the equation:

$$P(k) = P_{CDM} e^{-1/2k^2 R_f^2} \tag{4}$$

where R_f is the smoothing (filtering) scale and P_{CDM} is given by:

$$P_{CDM} = AkT^2(k) \tag{5}$$

where A is the normalization constant. We normalized the spectrum by imposing that the mass variance of the density field

$$\sigma^2(M) = \frac{1}{2\pi^2} \int_0^\infty dk k^2 P(k) W^2(kR) \tag{6}$$

convolved with the top hat window

$$W(kR) = \frac{3}{(kR)^3} (\sin kR - kR \cos kR) \tag{7}$$

of radius $8 \, h^{-1} \, Mpc^{-1}$ is $\sigma_8 = 0.76$ (Romano-Diaz et al. 2008). Throughout the paper we adopt a ΛCDM cosmology with WMAP3 parameters, $\Omega_m = 1 - \Omega_\Lambda = 0.24$, $\Omega_\Lambda = 0.76$, $\Omega_b = 0.043$ and $h = 0.73$, where h is the Hubble constant in units of $100 \, \text{km} \, s^{-1} \, Mpc^{-1}$. The density profile of an initial, pre-collapse halo, at early times, $\delta_i(x)$, is related to $\delta_0(x)$ by the linear growth factor $D(z)$ (Peebles 1980) by:

$$\delta_i(x) = \delta_0(x)/D(z_i) \tag{8}$$

Let us divide the main smooth spherically symmetric halo, $\delta(x)$, into many concentric mass shells. Each shell is uniquely labeled by x, its initial comoving radius. The halo represents an upward departure from average background density, i.e. density interior to any shell is greater than critical at all times. Each shells evolution is divided into two stages. Initially a shell expands with the Hubble flow, but with a slight deceleration arising from the central mass concentration. Eventually the shells outward radial velocity decreases to zero, after which the shell collapses, by some distance, back towards the center of the halo. The dividing moment is called the turn-around, and at any given time corresponds to the line dividing Regions (1) and (2). In a halo with a declining density profile the turn-around happens at progressively later cosmic times for shells at greater distances from the center.

---

[2] σ is the mass variance filtered on a scale R_f

In such cases the time evolution of a shell until it reaches turn-around is given by a set of parametric equations (Gunn & Gott 1972, Peebles 1980),

$$r(\theta) = \frac{1}{2} x \bar{\delta}_0^{-1}(1 - \cos\theta), \tag{9}$$

$$t(\theta) = \frac{3}{4} t_0 \bar{\delta}_0^{-3/2}(\theta - \sin\theta), \tag{10}$$

where r is particle's proper radius, t is cosmic time, and $\bar{\delta}_0(x)$ is the initial average fractional density excess inside the shell (Eq. [13] of RG87),

$$\bar{\delta}_0(x) = \frac{3}{x^2} \int_0^x \delta_0(y)\, y^2\, dy, \tag{11}$$

and t_0 is the present time. The mass of a shell, and the mass within a shell are constant; these relations, together with Eqs. 9 and 10 can be used to compute the fractional overdensity for any shell, parameterized by its $\delta_0/\bar{\delta}_0$, at a cosmic time corresponding to θ, (Eq. [23] of RG87):

$$\delta(\theta) + 1 = \frac{9(\theta - \sin\theta)^2}{2(1 - \cos\theta)^3}\left(1 + 3\left[1 - \frac{\delta_0}{\bar{\delta}_0}\right]\left[1 - \frac{3\sin\theta(\theta - \sin\theta)}{2(1 - \cos\theta)^2}\right]\right)^{-1}, \tag{12}$$

This can be used to construct the density run of a halo at a fixed cosmic time t/t_0.

The mean density distribution about a peak is spherically symmetric. However, the initial density peak will in general have a triaxial shape, leading to non-spherical collapse. As shown by R88a, since the quadrupole moment of the protogalaxy is largely due to the outermost shells, where triaxiality is insignificant, it is justifiable to ignore the triaxility in computations. In other terms, the dynamics of the halo collapse are dictated by the potential, which, being a double integral over all space, is much rounder than the mass distribution. Therefore the effects of intrinsic triaxiality of initial density peaks are smaller than those due to the secondary perturbations, and so can be ignored. Furthermore, initial triaxiality is less severe in larger, 2-4 σ peaks (Bardeen et al. 1986), which are the subject of the present study. With this caveat the smooth part of our density peak is still described by Eq. (1).

Moreover, in reality, the initial density peak will not be smooth, but will instead be sprinkled with many smaller scale positive and negative perturbations that arise from the same Gaussian random field that gave rise to the main peak. These secondary perturbations will perturb the motion of the dark matter particles from their otherwise purely radial orbits.

So, in order to investigate effects such as tidal torques and nonradial collapse, it is necessary to consider the nonspherical portion of the density distribution. In addition to the smooth halo, RG87 and Williams et al. (2004) considered contributions from the secondary perturbations which arise from the same Gaussian random field that gave rise to the main halo. The overall initial density profile, linearly evolved to the present day, can be written as,

$$\rho(\mathbf{x}) = \rho_0[1 + \delta_0(x)][1 + \epsilon_0(\mathbf{x})], \tag{13}$$

where ρ_0 is the present day background density, density excess due to the main halo is $\delta_0(x)$, and is assumed to be spherically symmetric, and $\epsilon_0(\mathbf{x})$ is the density excess contributed by the random secondary perturbations. In a statistical sense, the growth rate will depend on $\delta_0/\bar{\delta}_0$, or, equivalently, x, either of which can be used to parameterize the strength of the tidal field in a spherically symmetric halo. The final expression for the growth rate is given by (Eq. [28] of RG87 and Williams et al. 2004)

$$\epsilon(x, \theta) = \frac{\epsilon_0(x)}{\bar{\delta}_0} \frac{f_2(\theta)}{f_1(\theta) - [\delta_0(x)/\bar{\delta}_0(x)]f_2(\theta)}, \tag{14}$$

where $\epsilon_0(x)$ is the amplitude of the initial perturbation, given by

$$\epsilon_0(\mathbf{x}) = \frac{1}{(2\pi)^3} \int d^3k\, \epsilon_{\mathbf{k}}\, e^{i\mathbf{k}\cdot\mathbf{x}}, \qquad \langle|\epsilon_{\mathbf{k}}|^2\rangle = P(k) \tag{15}$$

and f_1 and f_2 are functions of the 'time' parameter θ: $f_1(\theta) = 16 - 16\cos\theta + \sin^2\theta - 9\theta\sin\theta$, and $f_2(\theta) = 12 - 12\cos\theta + 3\sin^2\theta - 9\theta\sin\theta$.

At any given time and proper position the random acceleration due to perturbation field $\epsilon(\mathbf{r})$ is given by (RG87 Eq. [40]):

$$\mathbf{g}(\mathbf{r}, t) = \mathbf{g}_{tot}(\mathbf{r}, t) - \mathbf{g}_b(\mathbf{r}, t) \approx G \int d^3 r' \frac{\rho_b(\mathbf{r}', t)\epsilon(\mathbf{r}, t)}{|\mathbf{r}' - \mathbf{r}|^3}(\mathbf{r}' - \mathbf{r}), \tag{16}$$

which is an integral over all space, and $\rho_b(\mathbf{r}, t) = \rho_0(t)[1 + \delta(\mathbf{r}, t)]$ is the background density due to the main halo, and is related to the total density given by Eq. 13 by, $\rho(\mathbf{r}, t) = \rho_b(\mathbf{r}, t)[1 + \epsilon(\mathbf{r}, t)]$; $\rho_0(t)$ is the average density of the Universe at epoch t. Remembering that the density distribution in the main peak and perturbation field and growth rate of perturbations are functions of radial position only, we use x instead of $\mathbf{x}$, and r instead of $\mathbf{r}$. Since, our goal is the *rms* value of acceleration, so scalar g will replace vector $\mathbf{g}$. A major simplification is accomplished by decoupling the time dependence of acceleration, i.e. the rate of growth of acceleration, from its spatial variation. Let the initial acceleration field due to secondary perturbations be denoted by $g_0(x)$. Then the dimensionless rate of growth of acceleration is given by,

$$F_g(x, t) = g(x, t)/g_0(x) = g(r, t)/g_0(r). \tag{17}$$

With these, the proper displacement of a particle can be evaluated as

$$d_p(x, t) = \int_0^t dt_1 \int_0^{t_1} dt_2 \, g(x, t_2) = g_0(x) \int_0^t dt_1 \int_0^{t_1} dt_2 \, F_g(x, t_2) = \Delta g_0(x) t_0^2 F_r(x, t), \tag{18}$$

Next we describe the two functions, $F_g(x, t)$ and $g_0(x)$, separately.

The acceleration growth rate becomes (RG87 Eq. [44][3])

$$F_g(x, \theta) = \frac{g(x, \theta)}{g_0(x)} = \frac{\rho_0[1 + \delta(x, \theta)]\epsilon(x, \theta)r(x, \theta)}{\rho_0\epsilon_0 x} = 8\bar{\delta}_0 \frac{f_2(\theta)}{[f_1(\theta) - \frac{\delta_0(x)}{\delta_0(x)} f_2(\theta)]^2}, \tag{19}$$

The spatial dependence of acceleration is given by:

$$\Delta g_0(d, x) = 4G\rho_0 \left[\int P_s(k)e^{-kd}(1 - \frac{\sin kx}{kx})dk\right]^{1/2}. \tag{20}$$

The comoving displacement is given by:

$$d(x, t) = d_p(x, t)/a(t) = \Delta g_0(x) t_0^2 F_r(x, t)/a(t). \tag{21}$$

In the early part of the evolution of the halo most of the shells are still expanding. During this time secondary perturbations grow, and so does the acceleration, the velocity, and the displacement contributed by these perturbations to the particles in the shell. Because the secondary peaks are randomly distributed within the halo, they displace the dark matter particles in random directions from their original positions. This can be visualized as a shell having an internal velocity dispersion, resulting in a "swollen" shell. If we concentrate on a single particle, its orbit, viewed from the rest frame of the parent shell, will oscillate between an inner and an outer radius of that shell (i.e. pericenter, r_p and apocenter, r_a). In general, this orbit will not be closed and will resemble a rosette. In a real situation, the "swell" of any given shell will gradually increase as the shell expands away from the center of the halo, and the influence of the secondary peaks grows, but for simplicity, as long as a given shell is expanding its dark matter particle positions and velocities are not corrected for the effects of secondary perturbations. So, the contributions are evaluated analytically but are not imparted to the shell until it reaches turnaround.

The magnitude of the extra velocity imparted to a typical dark matter particle at the time of turn-around (Eq. [48] of RG87),

$$|\Delta\mathbf{v}_{\mathrm{rms}}(x, t_c/2)| = F_v(x, t_c/2)\Delta g_0[d(x, t_c/2), x]t_0, \tag{22}$$

---

[3] Note a typo in their paper: $f_1(\theta)$ in the numerator of Eq. (44) should be $f_2(\theta)$.

where the velocity growth factor $F_v(x,t)$ is:

$$F_v(x,t) = \int_0^\theta F_g(x,\theta_1)\frac{dt}{d\theta_1}d\theta_1 \tag{23}$$

and the tangential, v_{tan}, and radial, v_{rad}, components of velocity are:

$$(\Delta v_{tan})^2 = \frac{2}{3}|\Delta\mathbf{v}_{\rm rms}(x)|^2, \quad \text{and} \quad (\Delta v_{rad})^2 = \frac{1}{3}|\Delta\mathbf{v}_{\rm rms}(x)|^2. \tag{24}$$

The mean radial velocity at $t = t_c/2$ is zero, while the mean tangential velocity is given by:

$$j_\theta(x) = \left(\frac{2}{3}\right)^{1/2} r_m \Delta v(x,t_c/2) \tag{25}$$

It is important to note that j_θ is inversely correlated with the height of the peak in δ, since both Δv and r_m (the maximum expansion radius) decrease with an increase in the height ν of the peak. The random angular momentum is important for the particle (shell) orbits since the larger it is, the larger is the orbital ellipticity, and then the shell penetrates less to the center, resulting in a flattening of the inner density profile. In several of the previously quoted papers (even Williams et al. 2004) only the random angular momentum was taken into consideration, while we take also account of ordered angular momentum, dynamical friction and adiabatic contraction.

The collapse starts from the inner most shell, the one adjacent to the core. When the first shell reaches its r_m it collapses and finds its r_a and r_p within the overall halo potential. It is assumed that the potential is changing slowly compared to the dynamical timescales of the shells, so that every shell conserves its adiabatic invariants, the radial and tangential momenta,

$$j_\theta(x) = \Delta v_{tan}\, r_m \tag{26}$$

$$j_r(x) = \int_{r_p}^{r_a} v_{rad}\, dr \tag{27}$$

throughout the collapse. This is an important assumption in the RG87 formalism, it is crucial to the computation of dynamics of shell crossing. Up to the moment when a given shell reaches its maximum expansion radius $r_m(x)$ at a time $t = t_c(x)/2$ corresponding to $\theta = \pi$, the shell is assumed to be thin, its radial extent determined by the initial shell separation. At r_m, the average dark matter particle in the shell is given its additional random velocity, Eq. 22 and Eq. 24. In either case the apocenter and pericenter can be calculated from the particle's energy integral and Δv_{tan} and Δv_{rad}. The energy integral,

$$E = \psi(r_m) - \frac{1}{2}\left[\left(\frac{dr}{dt}\right)^2 + \left(\frac{j_\theta}{r}\right)^2\right] \tag{28}$$

is conserved if ψ is not too rapidly changing with time, an approximation which is good outside the immediate region of the core.

The radial velocity of a particle is

$$v_{rad} = [2(E - \psi(r)) - (j_\theta/r)^2]^{1/2}, \tag{29}$$

(RG87). Note that RG87 define their energy integral and potential as the negatives of the conventional definitions of these quantities. We use the conventional definitions, i.e. potential is a negative quantity inside the halo, and energy integral of a bound particle is negative.

The addition of a random radial velocity ensures that the apocenter distance is greater than r_m, the radius of maximum expansion in the absence of velocity perturbations. A measure of the mean radial momentum of the particle is the radial action, (RG87):

$$j_r = \int_{r_p}^{r_a} v_r dr = \overline{v}_r dr(r_a - r_p) \tag{30}$$

The radial distribution of mass within a shell between apocenter and pericenter is not uniform. The density in the radial range dr around r is proportional to the amount of time the particle spends there, (Eq. [53] of RG87),

$$P(r)\,dr = \frac{v_{rad}^{-1}\,dr}{\int_{r_p}^{r_a} v_{rad}^{-1}\,dr}.$$ (31)

If M_{shell} is the mass of the added shell, then the total mass distribution of the core and shell together is:

$$M_1(r) = M(r) + M_{shell} \int_{r_p}^{r} P(r')dr'$$ (32)

From this mass function, the new potential $\psi_1(r)$ is calculated. The next mass shell is added and its probability distribution is calculated in the potential $\psi_1(r)$. However, the mass distribution of a newly added shell overlaps with shells which have fallen earlier; that is, the pericenter of the shell is at a smaller radius than the apocenters of some fraction of the previously added shells. Thus we must recompute after adding each new shell the orbits for each shell with which it overlaps. Since the potential is not violently changing, the adiabatic invariants of the orbits are conserved. In this case, the adiabatic invariants are the angular momentum j_θ and the radial action j_r. By repeatedly adding shells in this manner, while adjusting the orbits so that the angular momentum and radial action of the orbits are conserved, a self-consistent mass distribution is built up. [4]

The collapse of a perturbation taking into account angular momentum, and dynamical friction may be calculated by solving the equation for the radial acceleration (Kashlinsky 1986, 1987; Antonuccio-Delogu & Colafrancesco 1994; Peebles 1993):

$$\frac{dv_r}{dt} = \frac{h^2(r,\nu) + j^2(r,\nu)}{r^3} - G(r) - \mu\frac{dr}{dt}$$ (33)

where $h(r,\nu)$ is the ordered specific angular momentum generated by tidal torques, $j(r,\nu)$ the random angular momentum (see RG87), $G(r)$ the acceleration, and μ the coefficient of dynamical friction.

In the peculiar case of $\mu = 0$, Eq. (33) can be integrated to obtain the square of velocity:

$$v(r)^2 = 2\left[\epsilon - G\int_0^r \frac{m_T(y)}{y^2}dy + \int_0^r \frac{h^2}{y^3}dy\right]$$ (34)

where ϵ is the specific binding energy of the shell that can be obtained from the previous equation at turn-around when, $dr/dt = 0$.

If $\mu \neq 0$, the previous equation must be substituted with:

$$\frac{dv^2}{dt} + 2\mu v^2 = 2\left[\frac{h^2 + j^2}{r^3} - G\frac{m_T}{r^2}\right]v$$ (35)

which can be solved numerically for v. In the previous equation, we have two unknown quantities, the specific ordered angular momentum, h, and the coefficient of dynamical friction, μ.

The ordered angular momentum is connected to the tidal interaction of the proto-structure with the neighboring ones. The explanation of galaxies spins gain through tidal torques was pioneered by Hoyle (1949). Peebles (1969) performed the first detailed calculation of the acquisition of angular momentum in the early stages of protogalactic evolution. More recent analytic computations (White 1984, Hoffman 1986, R88; Eisenstein & Loeb 1995; Catelan & Theuns 1996) and numerical simulations (Barnes & Efstathiou

---

[4] In other words, the mass particles, once position and velocities are assigned, are allowed to follow the appropriate orbit in the gravitational potential of the previously collapsed matter. As each mass shell is added, those previously added shells with which it overlaps have their orbits adjusted so that the angular momentum j_θ and radial moments j_r integrated from pericenter to apocenter, are conserved.

1987) have re-investigated the role of tidal torques in originating the angular momenta of galaxies.

In the present paper, we take into account both types of angular momentum: random j, and ordered, h. As described in RG87, to calculate the ordered angular momentum, one has first to obtain the rms torque, $\tau(r)$, on a mass shell and then calculate the total specific angular momentum, $h(r, \nu)$, acquired during expansion by integrating the torque over time (Ryden 1988a (hereafter R88), Eq. 35):

$$h(r,\nu) = \frac{1}{3}\left(\frac{3}{4}\right)^{2/3}\frac{\tau_o t_0}{M_{sh}}\overline{\delta}_o^{-5/2}\int_0^\pi \frac{(1-\cos\theta)^3}{(\vartheta-\sin\vartheta)^{4/3}}\frac{f_2(\vartheta)}{f_1(\vartheta)-f_2(\vartheta)\frac{\delta_o}{\delta_o}}d\vartheta \qquad (36)$$

where $M_{sh} = 4\pi\rho_{\rm b}\left[1+\delta(x)\right]x^2\delta x$ is the mass in a thin spherical shell of internal radius x, τ_o is the tidal torque at time t_0, while the mean over-density inside the shell, $\overline{\delta}(r)$, is given by Eq. (11).

As remarked by Del Popolo et al. (2001) the angular momentum obtained from Eq. (36) is evaluated at the time of maximum expansion $t_{\rm m}$. With the BBKS power spectrum (filtered on a galactic scale), for a $\nu = 3$ peak of mass $\simeq 2\times 10^{11}M_\odot$, the model gives a value of $h = 2.5\times 10^{74}\,\frac{gcm^2}{s}$.

It is interesting to compare this result with a different method like that of Catelan & Theuns (1996), who calculated the angular momentum at maximum expansion time (see their Eqs. (31)-(32)) and compared it with previous theoretical and observational estimates. Assuming the same value of mass and ν used to obtain our previously quoted result and the same distribution of angular momentum as adopted by Catelan & Theuns (1996), we obtain a value for the angular momentum of $h = 2.0\times 10^{74}\,\frac{gcm^2}{s}$ in agreement with our result.

The total angular momentum of a system is often expressed in terms of the dimensionless spin parameter,

$$\lambda = \frac{L|E|^{1/2}}{GM^{5/2}}, \qquad (37)$$

where L is the angular momentum, summed over shells, and E is the binding energy of the halo. Expressing the values of angular momentum calculated as previously reported in terms of the spin parameter, we get a value of $\lambda \simeq 0.04$ for a 3σ peak of $\simeq 10^{12}M_\odot$[5]. This is comparable with values found in the literature (Barnes & Efstathiou 1987; Vivtska et al. 2002). Using the parameters in Vivitska et al. (2002), the maximum of the distribution of λ (well approximated by a log-normal distribution) is $\lambda = 0.035$ while there is a 90% probability that λ is in the range 0.02-0.1.

Since our paper deals also with LSB galaxies, we must recall that LSB galaxies are more angular momentum dominated compared to normal galaxies with the same luminosity (McGaugh & de Blok 1998). These galaxies are characterized by high values of λ: as shown in Boissier et al. (2002), 35% of all galaxies (in number) having $0.06 < \lambda < 0.21$ are LSBs. Therefore one expects according to several analytical papers (Nusser 2001; Hiotelis 2002; Le Delliou & Henriksen 2003; Ascasibar et al. 2004; Williams et al. 2004) that these objects should typically have shallower density cusps. Moreover the cores of these galaxies are much less dense than what the simulations indicate. In the case of LSB galaxies, we assumed a value of $\lambda = 0.06$ performing a conservative estimate. In agreement with what is reported, larger values of λ should imply a further flattening of the rotation curves in Fig. 3.

A more complete description of this calculation can be found in Del Popolo (2006).

It is important to note that after turn-around, not only the random angular momentum, j, will contribute to originate non-radial motions in the protostructure but also the ordered angular momentum, h. In fact, as successive shells expand to their maximum radius they acquire angular momentum and then fall in on orbits determined by the angular momentum. Actual peaks are not spherical; thus the infall of matter will not be purely radial. Random substructure in the region surrounding the peak will divert infalling matter onto non-radial orbits. The role of these random motions is of fundamental importance in structure formation.

---

[5] Notice that there is a very mild dependence of λ on peak height, or mass

We took into account dynamical friction by introducing the dynamical friction force in the equation of motions. In ordered to calculate μ, we recall that in hierarchical universes, matter is concentrated in lumps, and the lumps into groups and so on, which act as gravitational field generators. One can calculate the stochastic force generated by these field generators and then following Kandrup (1980) the dynamical friction force per unit mass

$$\mathcal{F} = -\mu v = -\frac{4.44[Gm_a n_{ac}]^{1/2}}{N} \log\left(1.12 N^{2/3}\right) \frac{v}{a^{3/2}} = -\beta_o \frac{v}{a^{3/2}} \tag{38}$$

where $N = \frac{4\pi}{3} R_{sys}^3 n_a$, is the total number of field particles, R_{sys} the system radius, m_a and n_a are respectively the average mass and the number density of the field particles, $n_{ac} = n_a \times a^3$ is the comoving number of field particles and a the expansion parameter, connected to the proper radius of a shell through:

$$r(r_i, t) = r_i a(r_i, t) \tag{39}$$

The number and mass of the field generators is then calculated using the theory of Gaussian random fields (BBKS). The acceleration obtained from Eq. (38) is used in the equation of motion. Again, the reader is referred to Del Popolo (2006) for a more complete description.

The shape of the central density profile is influenced by baryonic collapse: baryons drag dark matter in, causing the so called adiabatic contraction (AC) steepening the dark matter density slope. By considering a spherically symmetric protostructure, before dissipation, consisting of a baryonic fraction F with $F << 1$ of dissipational baryons and a fraction $1 - F$ of dissipationless dark matter particles constituting the halo, Blumenthal et al. (1986) described an approximate analytical model to calculate the effects of AC. One assumes that the dissipational baryons and the halo particles are well mixed initially (i.e., the ratio of their densities is F through the protostructure). This is due to the fact that the original angular momentum of the dark matter halo comes from gravitational (tidal) interactions with its environment. Thus, the dark matter and the gas experience the same torque in the process of halo assembly and should initially have (almost) the same specific angular momentum (Klypin et al. 2002). So, a usual assumption is that initially baryons had the same density profile as the dark matter (see the previous discussion and Mo et al. 1998; Cardone & Sereno 2005; Treu & Koopmans 2002; Keeton 2001).

In real systems, baryons assume a distribution in the central regions of the halo which is determined by the competition between dissipation and star formation. The dissipative infall of baryons will cease either when most of the baryon gas is converted to stars, ending dissipation, or when a rotationally supported gas disk is formed. As the baryons dissipate energy, they fall toward the center of the halo. If the baryons conserve their angular momentum as they fall inward, then the baryons will dissipate energy until they form a rotationally supported disk, whose shape is determined by the angular momentum distribution $h(M)$ of the baryons. So, summarizing, the two methods of ending dissipative infall result in a spheroidal distribution (if star formation ends the infall) or in a disk of stars (if angular momentum ends the infall) (R88a). So following the usual practice, the final baryon distribution is assumed to be a disk (for spiral galaxies) (Blumenthal et al. 1986; Flores et al. 1993; Mo et al. 1998; Klypin et al. 2002; Cardone & Sereno 2005). In our calculations, we shall assume the Klypin et al (2002) model for the baryon distribution (see their subsection 2.1), when dealing with mass scales typical of spiral galaxies. In the case of elliptical galaxies and clusters a typical assumption (that we shall use in the paper) is that baryons collapse to a Hernquist configuration (Rix et al. 1997; Keeton 2001; Treu & Koopmans 2002). One objection that one could advance is that clearly if the final baryon distribution is assumed to be a disk, the inner gravity potential is clearly non-spherical. The usual assumption that is made at this step (see RG87; R88a,b; Mo et al. 1998; Klypin et al. 2001; Cardone et al. 2006) is that the final configuration (in this case the disk) is assembled slowly, so that we can assume that the halo responds adiabatically to the modification of the gravitational potential and it remains spherical while contracting. The angular momentum of the dark matter particles is then conserved and a particle which is initially at radius r ends up at a rdius r', as described in the following.

The scale of the Hernquist profile is fixed by the competition between dissipation and star formation, when most of the baryon gas is converted to stars (see RG87; Gnedin et al. 2004).

We take into account adiabatic compression as done in RG87 improving it as done by Gnedin et al. (2004) (see the following). The Blumenthal et al. (1986), RG87, R88ab model for the adiabatic contraction can be described as follows. Since the baryon fraction F is much less than one, the adiabatic invariants of the dark matter orbits are conserved (Blumenthal et al. 1986; RG87). If the matter is on circular orbits, the invariant is $rM(r)$; if the dark matter is on radial orbits in a self-similar distribution, the invariant is $r_m M(r_m)$ (Blumenthal et al. 1986). Since the actual orbits are neither circular non radial, the two adiabatic invariants which are preserved are the angular momentum j_θ and j_r, of the orbits (RG87). In the absence of dissipation, the mass distribution $M_0(r)$ has a value of F which is constant throughout the structure. A self-consistent final solution, in which the baryons form a disk (or Hernquist configuration), conserving h, and the dark matter is compressed, conserving j_θ and j_r, is found by an iterative procedure. In the zeroth-order approximation, the baryons have their predissipation distribution $M_{B0} = FM_0(r)$, and the dark matter has the distribution $M_{D0} = (1 - F)M_0(r)$. While the dark matter distribution is held constant, the baryons fall inward, preserving their angular momentum until they are on circular orbits. Baryons originally at radius r and with specific angular momentum h will end up, in the stiff halo, at a radius,

$$r' = \frac{h^2}{G[M_{B0}(r) + M_{D0}(r')]}, \tag{40}$$

The baryons now have a new, more compact distribution $M_{B1}(r)$, and the central concentration of the baryons will draw the dark matter inward. The new potential of the baryons plus the dark matter is given by,

$$\Phi_1(r) = -G \int_r^\infty \frac{M_{D0}(s) + M_{B1}(s)}{s^2} ds, \tag{41}$$

After fixing the value of j_θ for each mass shell of the halo, the value of the apocenter is adjusted until the orbits of the dark matter in the potential $\Phi_1(r)$ have the same value of j_r, which they had in the predissipation distribution. The distribution of mass $M_{D1}(r)$ of the dark matter in the potential Φ_1 is built orbit by orbit, ensuring that j_θ and j_r are conserved. In the second iteration one has:

$$r'' = \frac{h^2}{G[M_{B1}(r) + M_{D1}(r'')]}, \tag{42}$$

and the new potential Φ_2 is calculated and the dark matter orbits are adjusted to preserve j_θ and j_r. The iteration continues till convergence. The previous model can be improved in two ways, as shown by Gnedin et al. (2004) and Klypin et al. (2002). It is worth stressing that there is some debate of the validity about the adiabatic compression formalism, with authors like Jesseit et al. (2002) finding a substantial agreement between the final dark matter distribution in numerically simulated haloes and that predicted by the adiabatic compression approach. On the other hand, this result has been contradicted on the basis of a set of higher resolution numerical simulations by Gnedin et al. (2004). According to these authors, the standard adiabatic compression formalism systematically overpredicts the dark matter density profile in the inner 5% of the virial radius, and the adiabatic compression formalism overpredicts the dark matter density less than $\simeq 10\%$ at r/r_v $\simeq 0.1$, while the error quickly decreases for larger values of r/r_v. Gustafsson et al. (2006) confirmed that the Blumenthal et al. (1986) model overestimates the central dark matter density. Moreover they showed that the modified model proposed by Gnedin et al. (2004) even if it is a considerable improvement it is not perfect. Moreover it is found that the contraction parameters in their model not only depend on the orbital structure of the dark-matter-only halos, but also on the stellar feedback prescription which is most relevant for the baryonic distribution. As a caveat we want to recall that according to Romano-Diaz et al. (2008), Gustafsson et al. (2006), even if focused on the AC, had an insufficient resolution to reach conclusive results. In the following, we shall take into

account the Gnedin et al. (2004) simple modification which describes numerical results more accurately than Blumenthal et al. (2006). They proposed a modified adiabatic contraction model based on conservation of the product of the current radius and the mass enclosed within the orbit-averaged radius,

$$M(\bar{r})r = \text{const}, \tag{43}$$

where the orbit-averaged radius is

$$\bar{r} = \frac{2}{T_r} \int_{r_p}^{r_a} r \frac{dr}{v_r}, \tag{44}$$

where T_r is the radial period, r_a is the apocenter radius and r_p the pericenter radius. The previous, classical AC model, assumes no angular momentum exchange between different components (e.g., baryons and dark matter), transfer of angular momentum from the baryons to the dark matter can be produced by dynamical friction, and the change of the AC model due to this effect can be taken into account by means of a simple model by Klypin et al. (2002).

For what concerns the universal baryon fraction, it has been inferred by observations involving different physical processes (Turner 2002). The power spectrum of matter inhomogeneities of large-scale structure is sensitive to the quoted F; the Two Degree Field Galaxy Redshift Survey has reported a value of 0.15 ± 0.07 (Percival et al. 2001). Measurements of the angular power spectrum of the CMBR also provide a very significant estimate. The combined analysis in Jaffe et al. (2001) of several data gives $F = 0.186^{+0.010}_{-0.008}$. By using Wmap collaboration data (Spergel et al. 2003) one obtains $F \simeq 0.16$ ($\Omega_b = 0.047 \pm 0.006$; $\Omega_m = 0.29 \pm 0.07$). After baryons cools and form stars, the baryon-to-total mass at the virial radius does not need to be equal to the previous quoted universal baryon fraction and may deviate from it depending on feedback effects, hierarchical formation details, and heating by the extragalactic UVB flux. In the AC calculation one has to take account that for large galaxies, only about half of the baryons, in principle available within the virial radius, goes into the central galaxy. For dwarf galaxies, this amount may be much smaller due to feedback effects, hierarchical formation details, and heating by the extragalactic UVB flux. In the following, in the case of large galaxies, we use one half of the universal baryonic fraction and for dwarfs values obtainable from Hoeft et al. (2007) (their Fig. 1). For example in the case of a dwarf galaxy of $10^{10} M_\odot$ it is about 0.06.

3. Results and discussion

After fixing the initial conditions and describing how to calculate angular momentum, dynamical friction and adiabatic contraction, we can use the model in Section 2 to obtain the density profile of haloes. In Fig. 1, we plot the profiles obtained through our model and those predicted by numerical simulations. In Fig. 1, the short-dashed line, the dashed line, and the solid line represents, respectively, the density profile for haloes of $10^{12} h^{-1} M_\odot$, $10^{10} h^{-1} M_\odot$, and $10^8 h^{-1} M_\odot$ calculated by means of the model of this paper. In order to compare the results of the model to those of N-body simulations, we plotted the NFW profile (dot-dashed line) for haloes having masses equal to $10^{12} h^{-1} M_\odot$, and $c = 10$, and the results for the same mass obtained in the Aquarius Project by Navarro et al. (2008) (upper dashed-lines). Navarro et al. (2008) showed that density profiles deviate slightly but systematically from the NFW model, and are better approximated by a fitting formula where the logarithmic slope is a power-law of radius: the Einasto profile,

$$\ln(\rho(r)/\rho_{-2}) = -2/\alpha[(r/r_{-2})^\alpha - 1], \tag{45}$$

where r_{-2} and ρ_{-2} are connected to the scaling radius and density of the NFW profile (see the following) by $r_{-2} = r_s$ and $\rho_{-2} = \rho_s/4$.

Density profiles become monotonically shallower inwards, down to the innermost resolved point, with no indication that they approach power-law behavior. The innermost slope they measure is slightly shallower than -1, a result supported by estimates of the maximum possible asymptotic inner slope. Shallower cusps, such as the $r^{-0.75}$ behavior

predicted by the model of Taylor & Navarro (2001), cannot yet be excluded. The NFW profile for the given mass was calculated by means of the relationships connecting the concentration parameter, c, and the virial mass, M_v, to the shape of NFW profile. We used the following equation for c,

$$c \simeq 13.6 \left(\frac{M_v}{10^{11} M_\odot} \right)^{-0.13}, \tag{46}$$

(Gentile et al. 2007), and the usual one for the NFW profile,

$$\rho(r) = \frac{\rho_s}{r/r_s(1 + r/r_s)^2} = \frac{\rho_b \delta_v}{r/r_s(1 + r/r_s)^2} \tag{47}$$

where

$$\delta_v = \frac{\Delta_v}{3} \frac{c^3}{\log(1 + c) - c/(1 + c)}, \tag{48}$$

and Δ_v is the virial overdensity (see Bryan & Norman 1998). The scaling radius, r_s, of the NFW profile is connected to the virial radius, concentration parameter and virial mass through $c = r_v/r_s$, where,

$$r_s \simeq 8.8 \left(\frac{M_v}{10^{11} M_\odot} \right)^{0.46} \text{kpc} \tag{49}$$

(Gentile et al. 2007). The residuals from the best Einasto fits are extremely small, and show no sign of systematic deviations down to the innermost resolved point. NFW residuals are then less than 30 % over the full radial range and below 20% within r_{-2}.

Figure 1 shows that halos generated using our method are different in character from the profiles predicted by numerical simulations, like those of NFW or the Aquarius Project. This result is not surprising since the types of evolution that numerical N-body and our halos undergo are rather different: the former are produced as a cumulative result of many minor and major mergers of smaller sub-halos, while the latter are the product of quiescent accretion of lumpy matter onto the primary halo. The NFW profiles change slope rapidly from $\alpha = 1$ to $\alpha = 3$ at the characteristic radius r_s. For example, in the case of the $10^{12} h^{-1} M_\odot$, the NFW profile have a characteristic scale length, equal to $0.1 r_v$, beyond which the density profile steepens, so that much of the mass is piled up within 10% of the virial radius. It is interesting to note that Navarro et al. (2004), Stadel et al. (2008) and the Aquarius Experiment start to show that the spherically-averaged density profile is not described, as in the NFW model just by an outer power-law $\rho \propto r^{-3}$ and inner power-law $\rho \propto r^{-1}$ but becomes progressively shallower inwards, and at the innermost resolved radius, the logarithmic slope is $\gamma \equiv -d \ln \rho/d \ln r \preceq 1$, ruling out claims of a steep $\rho \propto r^{-1.2}$ central cusp, and not excluding shallower cusps as the $r^{-0.75}$ behavior predicted by the model of Taylor and Navarro (2001). In other words, simulations with higher resolution are merging to the conclusion that the inner slope is not so steep as it appeared in less recent simulations and so in some cases even marginally consistent the DM halo of NGC 4605 ($\rho \propto r^{-0.65}$) (Simon et al. 2003). In the following, we discuss another reason why density profiles obtained in N-body simulations are different from those obtained in our model.

NFW profiles change slope rapidly from $\alpha = 1$ to $\alpha = 3$ at the characteristic radius r_s. For example, in the case of the $10^{12} h^{-1} M_\odot$ model, the NFW profile has a characteristic scale length, equal to $0.1 r_v$, beyond which the density profile steepens, so that much of the mass is piled up within 10% of the virial radius. The haloes obtained using the model in Section 2 are different in character from the profiles predicted by numerical simulations, like those of NFW. Within the virial radius the log-log density slope changes gradually and the slopes of the inner part of haloes flatten with decreasing mass. Our results show a steepening of the density profile with increasing mass with slopes $\alpha \simeq 0$ for $M \simeq 10^8 - 10^{10} h^{-1} M_\odot$, and $\alpha \simeq 0.8$ for $M \simeq 10^{12} h^{-1} M_\odot$. The profiles with $M \simeq 10^8 - 10^{10} h^{-1} M_\odot$ are well fitted by means of a Burkert's profile considered a good fit

to the dark matter rotation curves inferred from observations (e.g., Salucci & Burkert 2000). The functional form of this profile is characterized by,

$$\rho(r) = \frac{\rho_o}{(1 + r/r_o)[1 + (r/r_o)^2]},$$ (50)

where $\rho_o \simeq \rho_s$ and $r_o \simeq r_s$ (EZ01). The dark matter within the core is given by $M_o = 1.6\rho_o r_o^3$. Although the dark matter parameters r_o, ρ_o and M_o are in principle independent, the observations reveal a clear connection (Burkert 1995):

$$M_o = 4.3 \times 10^7 \, (r_o/kpc)^{7/3} \, M_\odot.$$ (51)

In panel (a) of Fig. 1, we plot the result of the model of this paper in the case baryonic infall is not taken into account, while in panel (b) baryonic infall is taken into account. Comparing panel (a) and (b), we observe that the presence of baryons leads to a steeper profile in agreement with previous studies (Blumenthal et al. 1986; Flores et al. 1993; Klypin et al. 2002; Gnedin et al. 2004; Gustafsson et al. 2006). It is important to note that the effect of baryonic infall is more evident at early redshifts, as shown in Fig. 5. As shown in Fig. 5, from $z = 3$ to $z = 2$ the profile becomes even steeper than the NFW cusp. Later the effect of angular momentum and dynamical friction reduces the slope and erases the cusp. However, as shown in Fig. 1 the initial steepening of the profile remains visible in the profiles calculated through the model of the present paper ($M \simeq 10^{12}h^{-1}M_\odot$, $M \simeq 10^{10}h^{-1}M_\odot$, and $M \simeq 10^8 h^{-1}M_\odot$), since the profile which takes into account baryonic infall (panel b) are steeper than those not taking it into account (panel a).

The model of the present paper gives just one profile for a given halo mass. In reality N-body simulations and analytical models different from those of Ryden-Williams and that of this paper (e.g. the extended Press-Schechter formalism), predict an ensemble of profiles for a given halo mass, depending on the different formation histories. For example, using the extended Press-Schechter (EPS) conditional probabilities for halo progenitor masses one can construct detailed histories of the mass assembly of dark matter haloes. One is interested in computing the mass accretion histories (hereafter MAHs) of dark matter haloes, defined as $\Psi(M_0, z) = M(z)/M_0$, where $M(z)$ is defined as the mass of the main progenitor halo, and M_0 is the halo mass at $z = 0$. One then defines the average mass accretion history of a halo of mass M_0 as,

$$\Psi(M_0, z) = 1/N \sum_{i=1}^{N} \Psi_i(M_0, z),$$ (52)

where the summation is over an ensemble of N random realizations (see van den Bosch & Frank 2002). One then can convert the mass growth curves $M(z)$ to density profiles as for example shown by Nusser & Sheth (1999). The single profile that we obtain in the present paper must be considered as the average profile of simulations.

Two important things must be noticed: a) less massive haloes are less concentrated; b) the halo's inner slope is smaller for smaller mass.

The first point can be explained as follows: higher peaks (larger ν), which are progenitors of more massive haloes, have greater density contrast at their center, and so shells do not expand far before beginning to collapse. This reduces j and h and allows haloes to become more concentrated. An alternative explanation is connected to the quoted angular momentum-density anti-correlation showed by Hoffman (1986): $j \propto \nu^{-3/2}$ (and similarly for h). So, density peaks having low (high) value of ν acquire a larger (smaller) angular momentum than high ν peaks and consequently the halo will be less (more) concentrated. It is important to notice that the quoted trend of increased central concentration as a function of mass applies only to halos that started out as peaks in the density field smoothed with a fixed R_f scale. Our conclusions do not mean that, for example, clusters of galaxies will be very much more centrally concentrated than galaxies, since different smoothing scales would apply in the two cases.

Point (b) can be explained in a similar way to (a), as described previously. Less massive objects are generated by peaks with smaller ν, which acquire more angular momentum (h and j). The angular momentum sets the shape of the density profile at the inner regions. For pure radial orbits, the core is dominated by particles from the outer shells. As the angular momentum increases, these particles remains closer to the maximum radius, resulting in a shallower density profile. Particles with smaller angular momentum will be able to enter the core but with a reduced radial velocity compared with the purely radial SIM. For some particles the angular momentum is so large that they will never fall into the core (their rotational kinetic energy makes them unbound). Summarizing, particles with larger angular momenta are prevented from coming close to the halo's center and so contributing to the central density. This has the effect of flattening the density profile. This result is in agreement with the previrialization conjecture (Peebles & Groth 1976; Davis & Peebles 1977; Peebles 1990), according to which initial asphericities and tidal interactions between neighboring density fluctuations induce significant non-radial motions that oppose the collapse. In order to reproduce the NFW profile, we performed an experiment similar to that performed by Williams et al. (2004), namely we reduced the magnitude of the h and j angular momentum, dynamical friction, μ and we considered the system as constituted only of dark matter ($F = 0$). The experiment was performed on the halo of mass $10^{12}h^{-1}M_\odot$, and in order to reproduce the NFW profile having $c = 10$ and mass $\simeq 10^{12}h^{-1}M_\odot$, we had to reduce the magnitude of h by a factor of 2, j and μ by a factor of 2.5. The result of the quoted experiment is the dashed line in Fig. 2, which closely reproduces the NFW profile (dot-dashed line), and the dotted line is the profile for the $10^{12}h^{-1}M_\odot$ halo obtained by means of our model.[6].

Similarly, Williams et al. (2004) had to reduce random velocities, which amount to reducing the angular momentum, in order to obtain a NFW profile. With each reduction of the random velocities, the profiles get steeper at the center. This effect can be understood, as already reported, as follows: the central density is built up by shells whose pericenters are very close to the center of the halo. Particles with larger angular momenta are prevented from coming close to the halo's center and so contributing to the central density. The correlation between increasing angular momentum and the reduction of inner slopes in halos has been also noticed by several other authors (Avila-Reese et al. 1998, 2001; Subramanian et al. 1999; Nusser 2001; Hiotelis 2002; Le Delliou & Henriksen 2003; Ascasibar et al. 2004). As previously mentioned, there could be, according to Williams et al. (2004) another reason of the difference of density profiles obtained from N-body simulations and models like that of this paper (or William's). As shown in their Fig. 1 (lower-left panel), the specific angular momentum distribution (SAM) in NFW-like halo is more centrally concentrated than the SAM distribution of the reference halo obtained with their model, model which is similar to that of this paper, and is closer to those of typical halos emerging from numerical simulations. This may suggest that haloes in N-body simulations lose a considerable amount of angular momentum between 0.1 and 1 r_v. Since virialization proceeds from inside out, this means that the angular momentum loss takes place during the later stages of the halos' evolution, rather then very early on. This is somehow confirmed by the so called angular momentum catastrophe, namely the fact that dark matter halos generated through gas-dynamical simulations are too small and have too little angular momentum compared to the halos of real disk galaxies, possibly because it was lost during repeated collisions through dynamical friction or other mechanisms (van den Bosch et al. 2002; Navarro & Steinmetz 2000). The problem can be solved invoking stellar feedback processes (Weil et al. 1998), but part of the angular momentum problem seems due to numerical effects, most likely related to the shock capturing, artificial viscosity used in smoothed particle hydrodynamics (SPH) simulations (Sommer-Larsen &Dolgov 2001).

We discussed the effect of changing the magnitude of angular momentum but we did not speak of the effect of changing the magnitude of μ (dynamical friction). The effect of changing this last quantity is very similar to changing the magnitude of angular momentum: an increase in the term μ produces shallower profiles as larger values of

---

[6] Note that the density profile of the Aquarius Experiment can be reproduced in the same manner with a small change in the h and j parameters used for the NFW profile.

angular momentum does. This is expected from Del Popolo (2006) (Fig. 1), showing that dynamical friction influence the dynamics of collapse in a similar way to that of angular momentum slowing down the collapse of outer shells and so compelling the particles to remain closer to the maximum radius.

At this point, we have to stress that the flattening of the density profile is caused by two main effects: angular momentum and dynamical friction. The other effect that we have considered, namely baryonic infall, counteracts the effect of the density profile flattening produced by angular momentum and dynamical friction. The role of baryonic infall is predominant at early times and produces a steepening of the profile, while later its effect is overwhelmed by the effect of angular momentum and dynamical friction. The result is similar to the one described by Williams et al. (2004) with the difference that in the present paper the effect of ordered angular momentum and dynamical friction adds to that of random angular momentum studied by Williams et al. (2004) with the result that the flattening of the density profiles is larger.

In Fig. 3, we plot the rotation curves obtained by our model and we compare them to four LSB galaxies shown in Williams et al. (2004). The four LSBs in Fig. 3 were taken from the high-resolution data of de Blok & Bosma (2002). Of the 26 LSBs that are presented in that paper we picked the ones with high inclination angles, smooth rotation curves, and good agreement between HI, Ha, and optical data. In all the four cases, the data are compared with the rotation curve obtained using our model (solid line) and with rotation curves obtained from NFW profile (dotted lines), given by,

$$V(r) = V_v \left\{ \frac{\ln(1+cx) - cx/(1+cx)}{x[\ln(1+c) - c/(1+c)]} \right\}^{1/2}. \tag{53}$$

where $x = r/r_v$ and V_v is the virial velocity [7]. The concentration parameter c was chosen to be consistent with the NFW predictions, calculating it from the mass of the galaxy through Eq. (46). For all the four galaxies the rotation curves obtained with the model of the present paper (solid lines) are a considerably better fit than NFW (dotted lines). Fig. 3 shows that NFW haloes are higher than the rotation curves obtained using our model, in which more massive haloes tend to be more centrally concentrated and have flatter rotation curves. Less massive haloes are less concentrated, and have slowly rising rotation curves. In contrast NFW rotation curves rise very steeply and as a consequence NFW fits to dwarf galaxy rotation curves have too low concentration parameters (van den Bosch & Swaters 2001) compared to N-body predictions. NFW fails to reproduce the velocities and the shape of the observed rotation curves, predicting too high velocities in the central part of haloes, and even leaving c as free parameter, instead of using Eq. (46), there is no appreciable improvement in the fit. Using Eq. (46), one obtains very low values of c. The result is similar to that described by Gentile et al. (2004): data are much better described by core-like profiles, like the Burkert profile generating flatter rotation curves,

$$V(r) = \left(\frac{2\pi G\rho_0 r_o^3}{r} \right)^{1/2} \left\{ \ln\left[(1+r/r_o)\sqrt{(1+(r/r_o)^2)}\right] - \arctan(r/r_o) \right\}^{1/2}, \tag{54}$$

Our rotation curves are very similar to those generated by the Burkert profile and the residuals and discrepant points for our rotation curves are close to that given in Gentile et al. (2004) for the Burkert's fit to their data.

Our halos appear to be a closer match to the halos of spiral and dwarf galaxies, than are N-body halos. This may indicate that the halos of real late-type disk galaxies undergo a formation scenario similar to the one depicted by our method, i.e. collapse proceeds through a quiescent accretion of lumpy material and minor mergers, rather than through a merger-driven formation process characteristic of fully hierarchical models.

Before going on, we notice that of the four rotation curves, NGC100 seems to be almost equally well fitted by the two type of models. In some other cases, the difference between the NFW rotation curves and those of the present paper is even smaller than

---

[7] The value of the characteristic velocity V_v of the halo is defined in the same way as the virial radius r_v.

for NGC100 and so it would be worthwhile to discuss halo-to-halo scatter. During the hierarchical assembly of dark matter haloes, the inner regions of early virialized objects often survive accretion onto a larger system, thus giving rise to a population of subhaloes. Depending on their orbits and their masses, these subhaloes therefore either merge, are disrupted or survive to the present day. To fully describe, in a statistical sense, the non-linear distribution of mass in the Universe, it is essential that halo substructure is taken into account. These subhalos appear ubiquitous in high resolution cosmological simulations and provide the source of fluctuations. One can study the evolution of halos under the influence of a generation of subhalos, while real halos grow continuously by accretion and mergers. Fluctuations due to subhalos in parent halos are important for understanding the time evolution of dark matter density profiles and the halo-to-halo scatter of the inner cusp seen in recent ultrahigh resolution cosmological simulations. This scatter may be explained by subhalo accretion histories: when we allow for a population of subhalos of varying concentration and mass, the total inner profile of dark matter can either steepen or flatten.

As noticed in the introduction, while on galactic scales a large number of studies predicts central cores and it seems that the cusp/core problem is a real problem not attributable to systematic errors in the data (de Blok, Bosma & McGaugh 2003), on cluster scales the situation is less clear with slopes ranging from $\alpha = 0.5$ (e.g. Sand et al. 2002; Sand et al. 2004) to $\alpha = 1.9$ (Arabadjis et al. 2002).

In order to study the problem on cluster scales, we have calculated the density profile evolution of dark matter and that of the total matter distribution for a halo of $\simeq 10^{14} h^{-1} M_{\odot}$.

We used the method of Sect. 2 to calculate the density profile and then we repeated the experiment shown in Sect. 3 to reproduce the NFW profile for the quoted mass that we considered as the initial condition. [8]

After we evolved this profile using the method of Sect. 2 and taking the redshift dependence in the model using the technique described in Del Popolo (2001) (the reader is referred to the quoted paper to have more insights). The goal was to study the evolution of a NFW profile similarly to El-Zant et al. (2001,2004), Tonini et al. (2006), Romano-Diaz et al. (2008).

Before showing the results, we recall that in real haloes angular momentum is lost in the final stages of collapse through the transfer of angular momentum from the subclumps to external material through dynamical friction (Quinn & Zurek 1988; R88b; Klypin et al. 2002). Once the baryons condense to form stars and galaxies, they experience a dynamical friction force from the less massive dark matter particles as they move through the halo. Energy and angular momentum is transferred to dark matter, increasing its random motion. Moreover, angular momentum acquired in the expansion phase gives rise to non-radial motions in the collapse phase. The spherical approximation that we use, which ignores the possibility of large substructure forming, neglects the transfer of angular momentum through the interactions of subclumps [9]. In the present paper, the effect of dynamical friction was just taken into account as an additive term in the equation of motion, Eq. (33), without changing the sphericall symmetry of the problem as done by Peebles (1993) and Del Popolo (2006). The effect of the dynamical friction term in the equation of motion is very similar to that of angular momentum: an increase in the term μ produces shallower profiles as larger values of angular momentum does. This is expected from Fig. 1 of Del Popolo (2006), showing that dynamical friction influences the dynamics of collapse in a similar way to that of angular momentum slowing down the collapse of outer shells and so compelling the particles to remain closer to the maximum radius.

Fig. 4a plots the evolution of a density profile of $10^{14} h^{-1} M_{\odot}$. The solid line represents the initial density profile at $z = 3$, which slightly steepens due to baryon settling

---

[8] We could have directly started from a NFW profile for the given mass calculated by means of the NFW fitting formula.

[9] An approximate analytical approach to the problem of exchange of angular momentum between the dark matter particles and infalling baryons has been developed by Klypin et al. (2002).

in virialized dark matter haloes (AC) (dot-short-dashed line) at $z = 2$. Moreover, angular momentum acquired in the expansion phase gives rise to non-radial motions in the collapse phase. The effect of angular momenta and dynamical friction overcomes that of the AC and the profile starts to flatten ($z = 1.5$ dotted line; $z = 1$ short-dashed line; $z = 0$ long-dashed line). The final dark matter profile (long-dashed line) is characterized by a log-log slope of $\alpha \simeq 0.6$ at $0.01r_s$. So the situation is similar to that of haloes on galactic scales but the slope is larger than for dwarf galaxies. In Fig. 4b, we plot the evolution of the total density profile at initial redshift, $z = 3$, (solid line) and at the final redshift $z = 0$ (dotted line). The plot shows that the total density profile slightly changes with time and the cusp is not "erased" as in the case of the dark matter profile. This result also implies that the baryonic component becomes steeper than the original NFW profile. The behavior of total mass is in agreement with X-ray observations by Chandra and XMM (Buote 2003, 2004; Lewis et al. 2003), weak lensing (Dahle et al. 2003) and strong lensing (Bartelmann 2003), which are consistent with a cusp having $\alpha = 1$ or larger. The behavior of the dark matter halo is in agreement with analysis of Sand et al. (2002, 2004) who fitted the baryonic and dark matter profiles only in the very inner part of the cluster MS 2137-23 within $\simeq 50h^{-1}$ kpc by means of a generalized NFW profile:

$$\rho(r) = \frac{\rho_b \delta_v}{(r/r_s)^\alpha (1 + r/rs)^{3-\alpha}} \tag{55}$$

obtaining a nearly flat core $\alpha = 0.35$. The steepening of the baryonic component is consistent with what found by Brunzendorf & Meusinger (1999), who found that the projected galaxy distribution in the Perseus cluster diverges as r^{-1}.

The results previously reported have several implications on the effort to test predictions of the CDM model observationally. The test that received much attention in the last decade, as several times stressed, is the density distribution in the inner regions of galaxies and clusters.

On galactic scales, as our results show, the infall of baryons at early times steepen the cusp due to AC (in agreement with previous studies: Blumenthal et al. 1986; Gnedin et al. 2004; Gustafsson et al. 2006) but later the cusp is erased through dynamical friction and non-radial motions effects. This results are in agreement with other analyses which study separately the effects of dynamical friction (e.g., EZ01) and those of angular momentum (non-radial motions) (e.g., Nusser 2001; Hiotelis 2002; Ascasibar et al. 2004; Williams et al. 2004) and with the recent Sph simulations of Romano-Diaz et al. (2008).

Going to larger scales the situation changes. The analysis of the density distribution for the bright galaxies is complicated by the uncertain contribution of stars to the total mass profile (Treu & Koopmans 2002; Mamon & Lokas 2004). Some analyses tend to favor inner slopes shallower than predicted by CDM (e.g., Gentile et al. 2004) but others deduce slopes of the inner profiles that are at least marginally consistent with predictions (Treu & Koopmans 2002, 204; Koopmans & Treu 2003; Jimenez et al. 2003). As previously reported, our results shows a steepening of the density profile with increasing mass with a density profile of haloes of mass $> 10^{12}h^{-1}M_\odot$ having slopes > 0.8. This is in agreement with recent N-body simulations having a logarithmic slope that decreases inward more gradually than the NFW profile (Hayashi et al. 2003; Navarro et al. 2004; Stadel et al. 2008). In the case of Stadel et al. (2008) the logarithmic slope is 0.8 at 0.05% of r_v.

The density distribution in clusters of galaxies can, in principle, provide a cleaner test of the models because the effects of the baryons and gas on the dark matter distribution are expected to be smaller and simpler. However also in this case observations predict slopes ranging from $\alpha \leq 0.5$ ($\alpha = 0.35$, Sand et al. 2002, 2004) to values larger than one (Arabadjis et al. 2002) with in some cases different results even for the same object. This is the case of the cluster MS2137-23 studied by Sand et al. (2004), who found a shallow density slope (≤ 0.5) while Dalal & Keeton (2003), Bartelman & Meneghetti (2004) and Gavazzi (2003) contested Sand's results, which according to them is neglecting lens ellipticity, and found consistency of the inner slope with a NFW profile. Our result concerning cluster scales makes a difference between dark matter and total mass distribution: the first tends to be less cuspy than the NFW profile in agreement with some observations (e.g., Sand et al. 2002, 2004), while the second is a bit more cuspy than the NFW profile (in agreement with Brunzendorf & Meusinger 1999) .

In the present paper, we did not take into account the baryon-DM interaction. As previously reported once the baryons condense to form stars and galaxies, energy and angular momentum is transferred to dark matter, increasing its random motion.

In future work, we will develop a semianalytic model to follow the evolution of the baryonic component, and its interaction with DM, and we will compare these with full hydrodynamical simulations. This should bring new insights into galaxy formation, and directly address possible small-scale challenges to the CDM theory. The role of the interaction between DM and baryons could bring further changes in the final density profile, that we shortly discuss. It is interesting to note that the problems of CDM only become clear on length scales where the baryons start playing a role and that this applies not only to the cusp/core problem but also to the missing dwarfs problem. Moreover, it is noteworthy that if, indeed, most starforming galaxies in the early universe lost their DM cusps because of stellar feedback, the missing dwarfs (satellites) problem could also be solved. Dwarf galaxies without a central cusp have a lower average core density than cuspy ones, and are hence much easier to disrupt tidally during the hierarchical assembly of larger galaxies (Mashchenko & Sills 2005). As a consequence, the removal of galactic cusps by stellar feedback in the early universe would result in fewer satellites today. This again indicates that baryon physics could be one of the missing pieces of the puzzle, and will very likely make a major contribution toward a solution. If this is true, it would be unwise to ignore the conclusions to which data are leading us, namely that small scales tells us more about galaxy formation than it does about CDM[10]. In other terms, the centers of galaxies are special places, the only places where we can study dark matter under peculiar conditions.

4. Conclusions

In this paper, we studied the cusp/core problem by improving the ESIM of Williams et al. (2004). We took into account, simultaneously, the effects of ordered and random angular momentum, dynamical friction and adiabatic contraction. The improved SIM of the present paper, taking account the previous effects gives rise to haloes being characterized by a log-log density slope that changes gradually within the virial radius and slopes of the inner part of haloes flattening with decreasing mass. As in previous papers, AC steepens the density profiles. The density profiles of structure having masses smaller than $10^{11}h^{-1}M_\odot$ are well fitted by Burkert's profiles. The comparison of some of the rotational curves given by de Blok & Bosma (2002) with the rotational curves obtained by means of our model, gives a good agreement. In the case of clusters of galaxies the density profile evolution is similar to that observed on galactic scales with the difference that the final slope is steeper than in the dwarf galaxies case. However the total mass profile is still cuspy and evolves slightly. The behavior of the dark matter halo is in agreement with the analysis of Sand et al. (2002, 2004) who fitted the baryonic and dark matter profiles only in the very inner part of the cluster MS 2137-23 within $\simeq 50h^{-1}$ kpc by means of a generalized NFW profile. The behavior of total mass is in agreement with X-ray observations by Chandra and XMM (Buote 2003, 2004; Lewis et al. 2003) weak lensing (Dahle et al. 2003) and strong lensing (Bartelmann 2003), which are consistent with a cusp having $\alpha = 1$ or larger. As also reported by Williams et al. (2004), numerically generated halos must have lost a considerable amount of their angular momentum in the outer parts, roughly between 0.1 and $1R_v$, possibly through dynamical friction or other mechanisms. A further future model taking into account the interaction between DM and baryons would help to better understand the problem.

References

Antonuccio-Delogu V., Colafrancesco S., 1994, ApJ 427, 72 (ADC)

---

[10] Other possibilities are that the observed dark matter cores are telling us that dark matter has pressure at small scales or something unexpected.

Arabadjis J. S., Bautz M. W., Garmire G. P., 2002, ApJ, 572, 66

Ascasibar Y., Yepes G., Gottlober S., 2004, MNRAS 352, 1109A

Ascasibar Y., Hoffman Y., Gottlöber S., 2007, MNRAS 376, 393

Avila-Reese V., Firmani C., Hernandez X., 1998, ApJ, 505, 37

Bardeen J.M., Bond J.R., Kaiser N., Szalay A.S., 1986, ApJ 304, 15

Barnes, J., Efstathiou, G., 1987, ApJ 319, 575

Bartelmann, M. 2003, in "Matter and Energy in Clusters of Galaxies", ASPC 301, 255

Bartelman M., Meneghetti M., 2004, A&A 418, 413

Bertschinger E., 1985, ApJS 58, 39

Blumenthal G. R., Faber S. M., Flores R., Primack J. R., 1986, ApJ, 301, 27

Boissier S., Monnier R. D., van Driel W., Balkowski C., Prantzos N., 2003, Ap&SS 284, 913

Borriello A., Salucci P., 2001, MNRAS, 323, 285

Bothun, G., Impey, C. & McGaugh, S. 1997, PASP, 109, 745

Bryan G. L., Norman M. L., 1998, ApJ 495, 80

Bullock, J.S., Dekel, A., Kolatt, T. S., Kravtsov, A.V., Klypin, A. A., Porciani, C. & Primack,
    J. R. 2001, ApJ, 555, 240

Brunzendorf, J. & Meusinger, H. 1999, Astron. & Astrophys. Suppl. Ser. , 139, 41

Buote, D. A. 2003, in "IGM/Galaxy Connection–The Distribution of Baryons at z=0",
    University of Colorado, 2003, ASSL Conference Proceedings Vol. 281, p. 87.

Buote, D. A. 2004, Proc. IAU 220, 149

Burkert A., 1995, ApJ, 447, L25

Cardone V. F., Sereno M., 2005, A&A 438, 545

Catelan P., Theuns T., 1996, MNRAS2 82, 436

Cen R., 2001, ApJ, 546, L77

Cen R. Y., Dong F., Bode P., Ostriker J. P., 2004, astro-ph/0403352

Cole S., Lacey C., 1996, MNRAS 281, 716

Colin P., Avila-Reese V., Valenzuela O., 2000, ApJ 542, 622

Dahle H., Hannestad S., Sommer-Larsen J., 2003, ApJ, 588, L73

Dalal N., Keeton C. R., 2003, astro-ph/0312072

Davis M., Peebles P.J.E., 1977, ApJS, 34, 425

Davé R., Spergel D. N., Steinhardt P. J., Wandelt B. D., 2001, ApJ, 547, 574

de Blok, W. J. G., McGaugh, S. S., Bosma, A., & Rubin, V. C. 2001a, ApJ, 552, L23

de Blok, W. J. G., McGaugh, S. S., & Rubin, V. C. 2001b, AJ, 122, 2396

de Blok, W. J. G., Bosma, A., & McGaugh, S. 2003, MNRAS 340, 657

de Blok W. J. G., McGaugh S. S., Bosma A., Rubin V. C., 2001, ApJ 552, L23

de Blok W. J. G., Bosma A., 2002, A&A 385, 816

de Blok W. J. G., 2003, in dark matter in Galaxies, ASP Conference series, Vol. 220, 2003, S.
    Ryder, D. J. Pisano, M. Walker, and K. C. Freeman, eds.

Del Popolo A., Gambera M., Recami E., Spedicato E., 2000, A&A 353, 427 (DP2000)

Del Popolo A., 2006, A&A 454, 17

Dubinski J., Carlberg R., 1991, ApJ 378, 496

Eisenstein D.J., Loeb A., 1995, ApJ 439, 250

El-Zant A., Shlosman I., Hoffman Y., 2001, ApJ, 560, 636 (EZ01)

El-Zant A., Hoffman Y., Primack J., Combes F., Shlosman I., 2003, ApJ, 2004, ApJ 607, 75

Ettori S., Fabian A. C., Allen S. W., Johnstone R. M., 2002, MNRAS, 331, 635

Filmore J.A., Goldreich P., 1984, ApJ 281, 1

Flores R. A., Primack J. R., 1994, ApJ, 427, L1

Flores R., Primack J. R., Blumenthal, G. R., & Faber, S. M. 1993, ApJ 412, 443

Fukushige T. & Makino, J, 2001, ApJ 557, 533

Fukushige T., Kawai A., Makino J. 2004, ApJ 606, 625

Ghigna S., Moore B., Governato F., Lake G., Quinn T., Stadel J., 2000, ApJ, 544, 616

Gavazzi R., 2003, in Impact of Gravitational Lensing on Cosmology Proceedings IAU Symposium
    N. 225, Mellier Y., & Meylan G. eds.

Gelato S., Sommer-Larsen J., 1999, MNRAS 303, 321

Gentile G., Salucci P., Klein U., Vergani D., Kalberla P., 2004, MNRAS 351, 903

Gentile G., Tonini C. & Salucci P., 2007, MNRAS 378, 41

Gnedin, O. Y., Kravtsov A. V., Klypin A. A., Nagai D., 2004, ApJ 616, 16

Goodman J., 2000, New Astronomy 5, 103

Gott J.R., 1975, ApJ 201, 296

Gunn J.E., Gott J.R., 1972, ApJ 176, 1

Gunn J.E., 1977, ApJ 218, 592

Hayashi E., Navarro J. F., Power C., Jenkins A., Frenk C. S., White S. D. M., Springel V.,
    Stadel J., Quinn T. R., 2004 MNRAS, 355, 794

Henriksen R. N., Widrow L. M., 1999, MNRAS 302, 321

Hiotelis, N. 2002, A&A 383, 84

Hoeft M., Mucket J. P., Gottlober S., 2004, ApJ 602, 162

Hoffman, Y., 1986, ApJ 301, 65

Hoffman Y., Shaham J., 1985, ApJ 297, 16 (HS)

Hoyle, F.: (1949), in IAU and International Union of Theorethicaland Applied Mechanics Symposium, p. 195

Hozumi S., Burkert A., Fujiwara T., 2000, MNRAS 311, 377

Hu W., Barkana R., Gruzinov A., 2000, Physical Review Letters, 85, 1158

Jimenez R., Verde L., Oh S. P., 2003, MNRAS 339, 243

Jing, Y. P. & Suto, Y. 2000, ApJ, 529, L69

Kandrup, H.E., 1980, Phys. Rep. 63, n 1, 1

Kaplinghat M., Knox L., Turner M. S., 2000, Physical Review Letters, 85, 3335

Kashlinsky A., 1986, ApJ, 306, 374

Kashlinsky A., 1987, ApJ, 312, 497

Keeton C. R., 2001, ApJ 561, 46

Klypin, A., Kravtsov, A. V., Bullock, James S. & Primack, J. R. 2001, ApJ, 554, 903

Klypin A., Zhao H., & Somerville R. S. 2002, ApJ 573, 597

Koopmans L. V. E., Treu T., 2003, ApJ 583, 606

Kravtsov A. V., Klypin A. A., Bullock J. S., Primack J. R., 1998, ApJ, 502, 48

Le Delliou M., Henriksen R. N., 2003, A&A 408, 27

Lemson, G., 1995, Ph.D. thesis, Rïksuniversiteit Groningen

Lewis A. D., Buote D. A., Stocke J. T., 2003, ApJ 586, 135

Mamon G.A., Lokas E. L., MNRAS 2005, 362, 95

Marchesini D., DOnghia E., Chincarini G., Firmani C., Conconi P., Molinari E., Zacchei A., 2002, ApJ, 575, 801

Mashchenko S., Couchman H. M. P., Wadsley J., Nature 442, 539

Mashchenko S. & Sills, 2005, ApJ 619, 258.

Merrit D., Navarro J. F., Ludlow A., Jenkins A., 2005, ApJ 624, L85

Mo H. J., Mao S., & White S. D. M. 1998, MNRAS 295, 319

Moore B., 1994, Nature, 370, 629

Moore, B., Governato, F., Quinn, T., Stadel, J. Lake, G. 1998, ApJ, 499, L5

Navarro J.F., Frenk C.S., White S.D.M., 1995, MNRAS 275, 720

Navarro J.F., Frenk C.S., White S.D.M., 1996, ApJ 462, 563

Navarro J.F., Frenk C.S., White S.D.M., 1997, ApJ 490, 493 (NFW)

Navarro J. F., Hayashi E., Power C., Jenkins A. R., Frenk C. S., White S. D. M., Springel V., Stadel J., Quinn T. R, 2004,MNRAS 349, 1039

Nusser A., Sheth R. K., 1999, MNRAS, 303, 685

Nusser A., 2001, MNRAS 325, 1397

Peebles, P. J. E., 1969, ApJ 155, 393

Peebles P.J.E., Groth E.J., 1976, A&A 53, 131

Peebles P.J.E., 1980, The large scale structure of the Universe, Priceton University Press

Peebles, P.J.E., 1990, ApJ 365, 27

Peebles P. J. E., 2000, ApJ 534, L127

Power, C., Navarro, J. F., Jenkins, A., Frenk, C. S., White, S. D. M., Springel V., Stadel J., Quinn T., 2003, MNRAS 338, 14

Quinn P.J., Salmon J.K., Zurek W.H., 1986, Nature, 322, 329

Rhee G., Valenzuela O., Klypin A., Holtzman J., Moorthy B., 2004, ApJ 617, 1059

Ricotti M., 2003, MNRAS 344, 1237

Ricotti M., Wilkinson M. I., 2004, MNRAS 353, 867

Ricotti M., Pontzen A., Viel M., 2007, ApJ 663, 53

Rix, Hans-Walter; de Zeeuw, P. Tim; Cretton, Nicolas; van der Marel, Roeland P.; Carollo, C. Marcella, 1997, ApJ 488, 702

Romano-Diaz E., Shlosman I., Hoffman Y., Heller C., 2008, astro-ph 0808.0195

Ryden B.S., Gunn J.E., 1987, ApJ 318, 15 (RG87)

Ryden, B.S., 1988a, ApJ 329, 589 (R88)

Ryden, B.S., 1988b, ApJ 333, 78

Salucci P., Burkert A., 2000, ApJ 537, L9

Sand D. J., Treu T., Ellis R. S., 2002, ApJ 574, L129

Sand D. J., Treu T., Smith G. P., Ellis R. S., 2004, ApJ 604, 88

Simon J. D., Bolatto A. D., Leroy A. Blitz L., 2003b, in Satellites and Tidal Streams, ASP conference Series 2003

Stadel J., Potter D., Moore B., Diemand J., Madau P., Zemp M., Kuhlen M., Quilis V, 2008, astro-ph/0808.2981

Sommer-Larsen J., Dolgov A., 2001, ApJ 551, 608

Spekkens K. Giovanelli R., Haynes M. P., 2005 AJ 129, 2119

Spergel D .N., et al. 2003, ApJS 148, 175

Spergel D. N., Steinhardt P. J., 2000, Physical Review Letters 84, 3760

Subramanian K., Cen R., Ostriker J. P., 2000, ApJ 538, 528

Taylor J. E., Navarro J. F., 2001, ApJ 563, 483

Taylor J. E., Silk J., Babul A., 2004, IAUS no. 220, p. 91

Treu T. & Koopmans L. V. E., 2002, ApJ 575, 87

Treu T. & Koopmans L. V. E., 2004, ApJ 611, 739

van den Bosch, F. C., & Swaters, R. A. 2001, MNRAS325, 1017

van den Bosch, F. C., Robertson, B. E., Dalcanton, J. J., & de Blok, W. J. G. 2000, AJ 119, 1579

Yoshida N., Springel V., White S. D. M., Tormen G., 2000, ApJ 544, L87

White, S. D. M., 1984, ApJ 286, 38

White S.D.M., Zaritsky D., 1992, ApJ 394, 1

Williams L. L. R., Babul A., Dalcanton, J. J., 2004, ApJ 604, 18
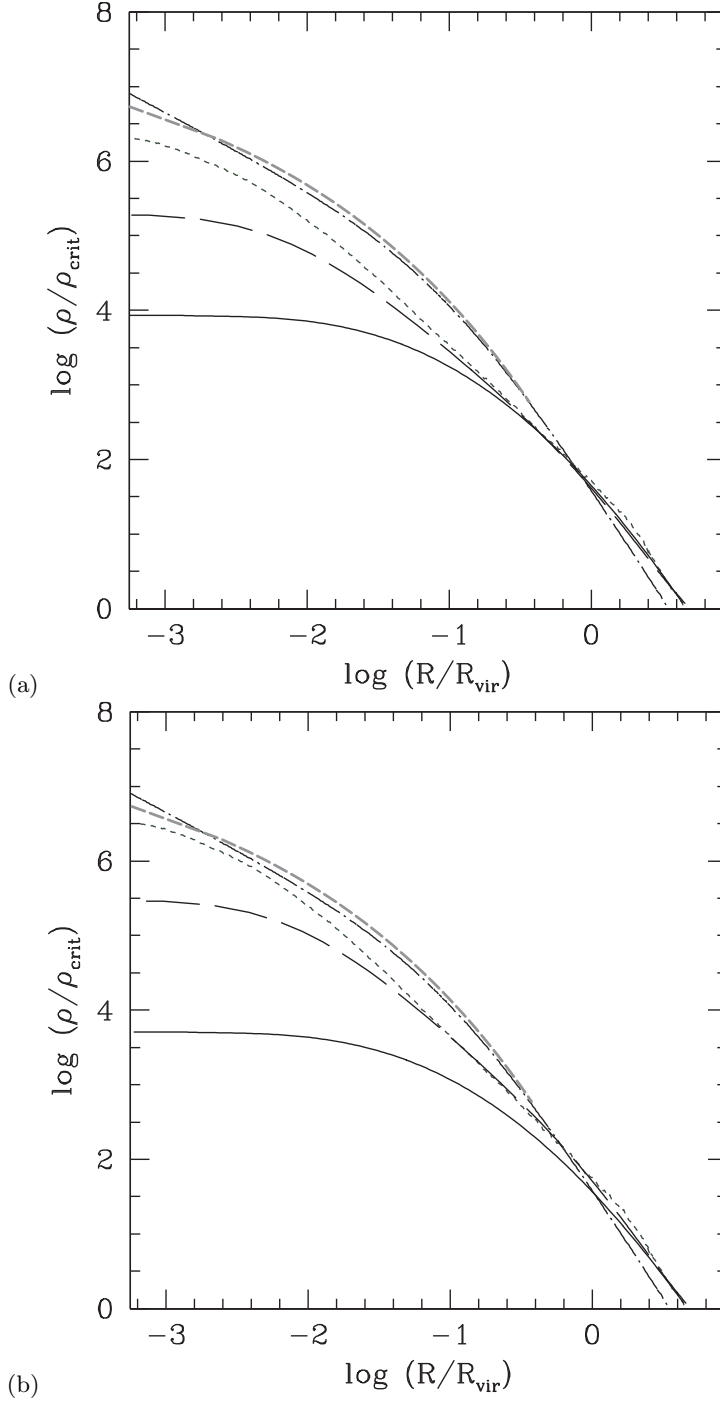
Fig. 1. Panel (a). Dark matter haloes generated with the model of Section 2. In this case we do not take into account baryon collapse. The upper dashed-line represents the results of the Aquarius Experiment for a halo of $M \simeq 10^{12} h^{-1} M_\odot$, the dot-dashed line represents the NFW profile for $c = 10$, calculated by means of Eqs. (46),(47), (48) expressing the scaling radius r_s in terms of the virial radius. The short-dashed line, dashed line and solid line represent, respectively, the density profile obtained by means of the model of the present paper for $M \simeq 10^{12} h^{-1} M_\odot$, $M \simeq 10^{10} h^{-1} M_\odot$, and $M \simeq 10^8 h^{-1} M_\odot$ without inclusion of baryonic infall. Panel (b) same of panel (a) but taking account of baryonic infall.
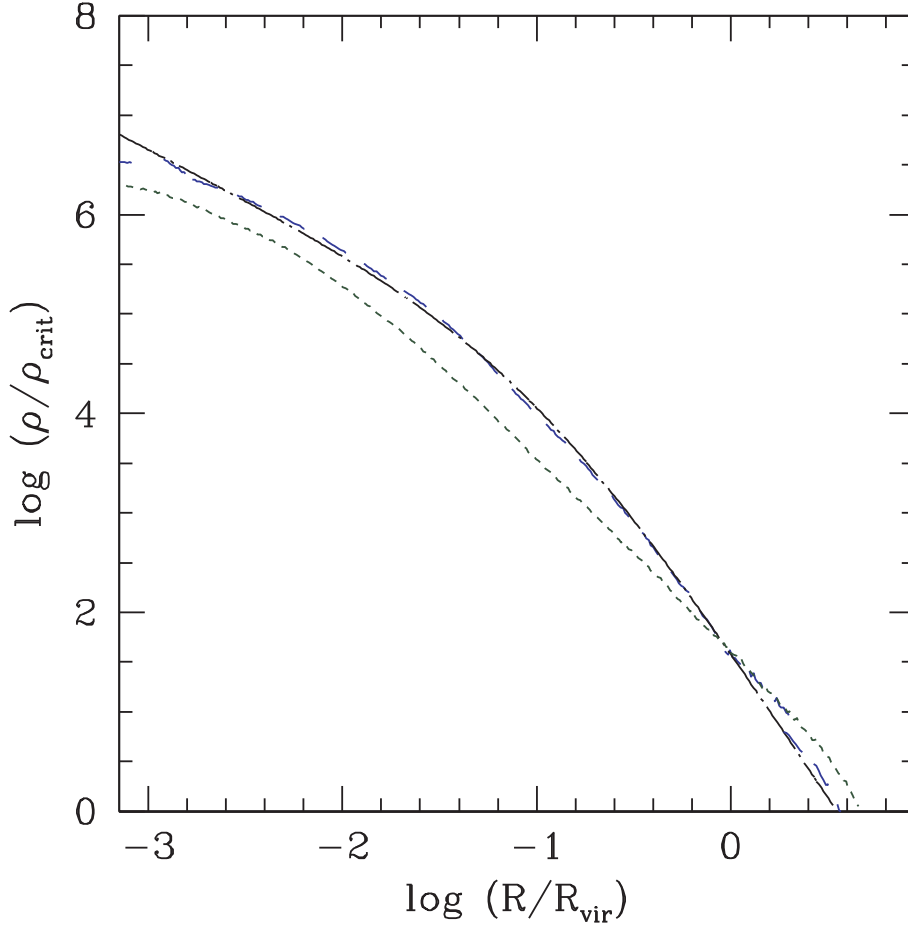
Fig. 2. Dark matter haloes generated with the model of Section 2. The dotted-dashed line is the NFW profile, the short-dashed line is the profile for the $10^{12}h^{-1}M_\odot$ halo obtained by means of our model. The dashed line represents the density profile obtained from the $10^{12}h^{-1}M_\odot$ halo by reducing the magnitude of h, j and μ as described in the text.
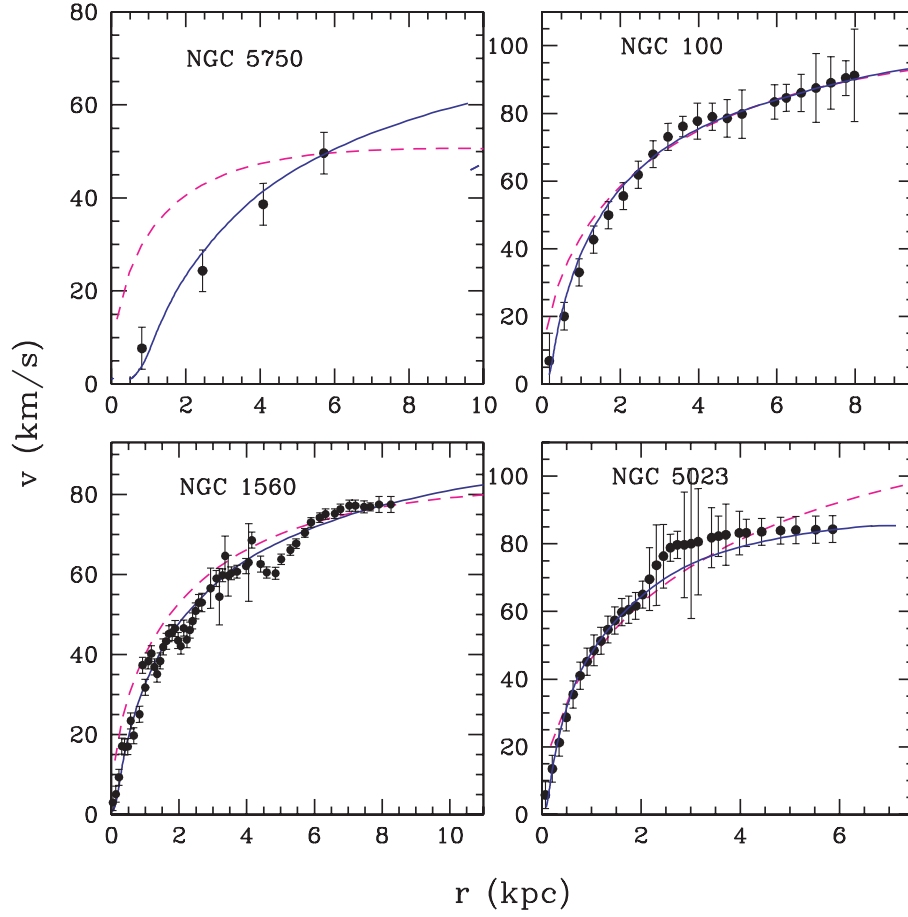
Fig. 3. Comparison of the rotation curves obtained with the model in Section 2 (solid lines) with the rotation curves of four LSB galaxies studied by de Blok & Bosma (2002). The dashed line represents the fit with NFW model (see Section 3 for details).

(a)

(b)
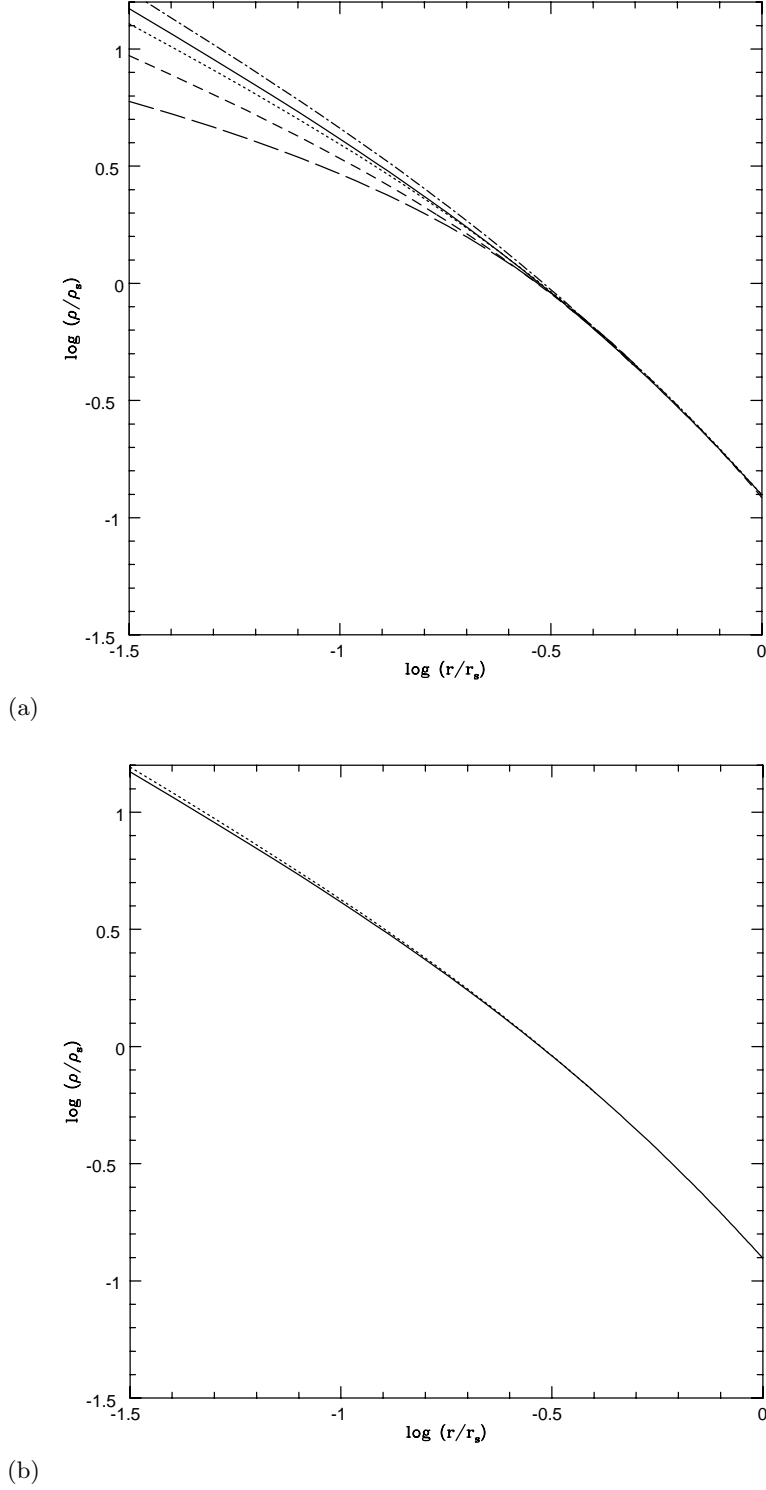
Fig. 4. Panel (a) Density profile evolution of a $10^{14}h^{-1}M_\odot$ halo. The solid line represents the NFW initial profile at $z = 3$. Notice how the baryonic infall at redshift $2 < z < 3$ steepens the NFW cusp. The profile at $z = 2$, $z = 1.5$, $z = 1$ and $z = 0$ is represented by the dot-short-dashed line, dotted line, short-dashed line, and long-dashed line respectively. Panel (b). Density profile evolution of a $10^{14}h^{-1}M_\odot$ halo for the total mass. The solid line represents the NFW initial profile at $z = 3$. The profile at $z = 0$ is represented by the dotted line.